High-Cycle Fatigue Properties of Ni-Baced Alloy718 and Iron-Baced A286 Supperalloys at Elevated-Temperature

K. Kobayashi [1], M. Hayakawa [1]and M. Kimura [1]
[1] *National Institute for Materials Science, Tsukuba, Japan*

Abstract

High-temperature fatigue properties of austenitic superalloys 718, A286 and 304L were investigated in region between 10^2 and 10^7 cycles. The alloys 718 and A286 are precipitation-hardening type austenitic superalloys, and 304L is a solid solution-hardening type austenitic steel.

The fatigue strengths of alloys 718 and A286 in high-cycle region over 10^4 cycles grain size effect. The initiation sites of the fracture were the crystallographic facets corresponding to the austenitic grain size.

Therefore the coarse-grain alloys showed the lower fatigue strength than the fine-grain alloys, because the fatigue strength is generally inversely proportionate to the initiation defect areas for the fatigue cracks. In low-cycle region under 10^4 cycles, on the other, the initiation sites of the fracture were the surface of the specimens. This type fracture mode is common for fatigue fracture of smoothed specimens.

The ratio of the fatigue limit at 10^7 cycles to the tensile strength is extremely low for the coarse-grain alloys compared with the common case of 0.5. From these results fatigue fracture map is proposed.

Key words: High-cycle fatigue properties; Austenitic superalloys; Fatigue fracture map.

1. Introduction

Alloys 718 and A286 are typical austenitic superalloys of the precipitation-hardening type, which are nickel-based and iron-based, respectively. They are used in high-temperature applications such as blades, disks, and the shafts of jet engines and gas turbines. Austenitic 304L stainless steel is also commonly used in high-temperature applications, but is a solid solution-hardening type. The above alloys and the steel are used in the main engine components of the Japanese space rocket H-IIA.

The National Institute for Materials Science (NIMS) and the Japan Aerospace Exploration Agency (JAXA) have been conducting the Data Sheet Project to produce fatigue strength data on space-use materials[1)]. These data have been published as NIMS Space Use Materials Strength Data Sheet Nos. 4, 6 and 7, for alloy 718, alloy A286 and 304L steel, respectively[2), 3), 4)].

This paper is a trial to understand the high-cycle fatigue strength of austenitic steel and superalloy from the viewpoint of austenitic gain size and tensile strength. Both fine and coarse-grain versions of alloys 718 and A286 were prepared and subjected to high-cycle fatigue tests.

2. Experimental methods

2.1 Materials

The list of materials used in this study and their chemical composition, processing, thermal history and grain size are shown in Table 1. In general, rolling produces fine-grain material and forging produces the coarse-grain material for alloys 718 and A286. Alloy 718 was subjected to a double aging heat treatment to enhance the precipitation of Ni_3Nb and alloy A286 was subjected to aging to precipitate Ni_3Al. The 304L steel was solution-treated only.

Figure 1 shows the microstructures of the materials.

The tensile properties of the materials at high temperatures are shown in Table 2.

Table 1 Chemical compositions (mass %) and processing details for materials used.

Materials	C	Si	Mn	P	S	Ni	Cr	Mo	V	Co	Cu	Ti	Al	B	Fe	Nb	Ta
Coarse grain alloy 718	0.032	0.09	0.12	0.006	0.0001	53.6	18.64	2.95	--	0.15	0.04	1.02	0.479	--	18.05	5.11	0.017
Fine grain alloy 718	0.023	0.03	0.03	0.002	0.0017	52.3	18.00	3.18	--	0.02	0.005	0.98	0.49	--	19.5	5.35	--
Coarse grain alloy A286	0.04	0.14	0.16	0.011	0.004	25.01	14.44	1.32	0.33	0.34	0.04	2.06	0.17	0.0033	bal.	--	--
Fine grain alloy A286	0.032	0.55	1.14	0.020	0.004	24.65	13.91	1.27	0.15	--	0.14	2.50	0.26	0.0078	bal.	--	--
Coarse grain 304L steel	0.021	0.64	1.79	0.011	0.002	9.55	18.62	0.15	--	--	0.25	--	--	--	--	--	--

Materials	Processing and product form	Thermal history	Grain size(μm)
Coarse grain alloy 718	forging, rolling, plate	Solution treatment: 1045℃, 1h→ Air cooling Aging: (720℃, 8h→ Furnace cooling 620℃, 10h → Air cooling) * 2	100-200
Fine grain alloy 718	rolling, bar	Solution treatment: 960℃, 1h→ Air cooling Aging: 720℃, 8h→ Furnace cooling 620℃, 8h → Air cooling	10-20
Coarse grain alloy A286	forging, billet	Solution treatment:980℃, 2h→ Oil quenching Aging: 718℃, 16h →Air cooling	120
Fine grain alloy A286	rolling, bar	Solution treatment: 982℃, 1h→ Water quenching Aging: 715℃, 16h →Air cooling	20
Coarse grain 304L steel	forging, billet	Solution treatment: 1030℃, 70min→ Water cooling or oil cooling	125

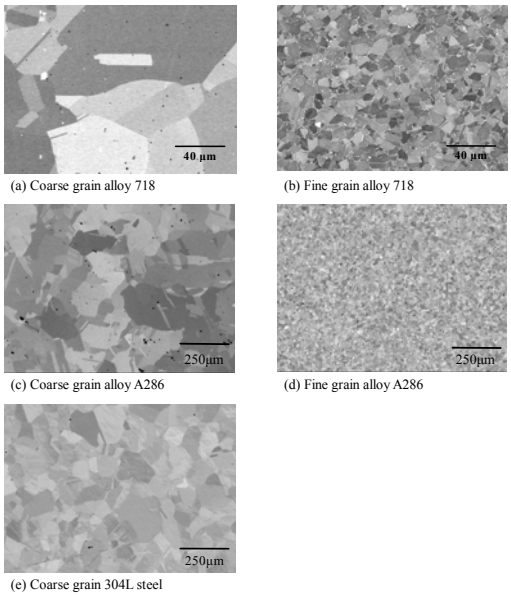

(a) Coarse grain alloy 718 (b) Fine grain alloy 718

(c) Coarse grain alloy A286 (d) Fine grain alloy A286

(e) Coarse grain 304L steel

Figure 1 Microstructures of materials used.

Table 2 High-temperature tensile properties of materials used.

Materials	Temperature (℃)	0.2% proof stress (MPa)	Tensile strength (MPa)	Elongation (%)
Coarse grain alloy 718	600	956	1089	21
Fine grain alloy 718	550	1042	1212	21
Coarse grain alloy A286	600	593	837	19
Fine grain alloy A286		713	912	22
Coarse grain 304L steel	500	109	364	44

2.2 Fatigue tests

Axial load-controlled fatigue tests were conducted using servo-hydraulic fatigue-testing machines. The wave shape was sinusoidal, and the frequency was 10 Hz. The fatigue tests were continued up to 10^7 cycles. The fatigue specimens were of the hourglass type or the cylindrical parallel type, with diameters of 6 or 3 mm depending on the sizes of the materials and the capacities of the testing machines.

The test condition of stress ratio ($R = \sigma_{min}/\sigma_{max}$) and temperature was determined by considering the parts of the HIIA rocket engines in which the materials were used, where σ_{min} and σ_{max} are the minimum and maximum stresses of the sinusoidal wave, respectively. The details of the test conditions are listed in Table 3. The specimens were heated in electric furnaces.

Table 3 Fatigue test condition of stress ratio and temperature.

Materials	Stress ratio	Temperature (℃)
Coarse grain alloy 718	-1	600
Fine grain alloy 718		550
Coarse grain alloy A286	-1 and 0.01	600
Fine grain alloy A286		
Coarse grain 304L steel	0.01	500

3. Results

Results of the fatigue tests for the alloys 718, A 286 and the 304L steel are shown in Figures 2, 3, and 4, respectively.

A distinct gain size effect on the fatigue strength was observed, especially in the high-cycle region for alloy 718, shown in Figure 2, even though the testing temperatures varied somewhat. The temperature difference of 50 ˚C is not a reason, however, for the difference in the fatigue strength between the fine and coarse versions, since the difference in the fatigue strength is not normalized by the difference in the tensile strength. In this case the stress ratio R is –1.

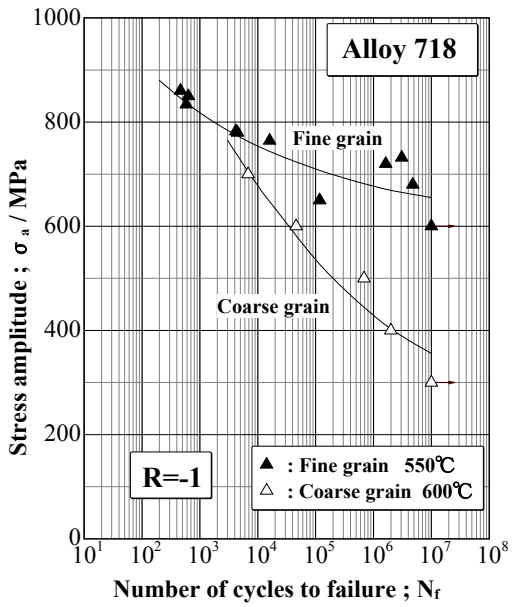

Figure 2 Fatigue strengths for the fine and the coarse-grain versions of alloy 718.

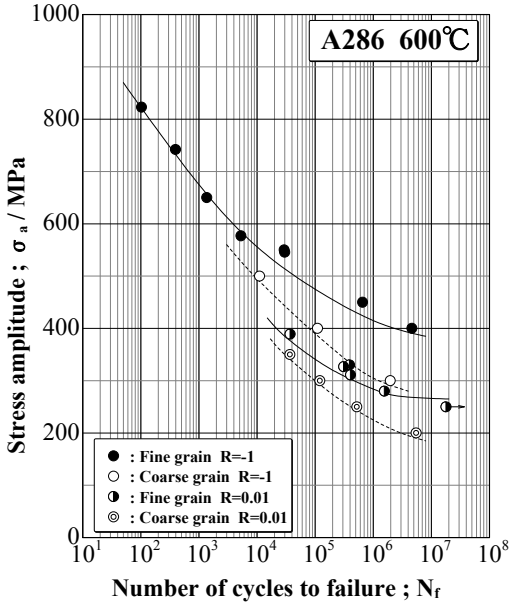

Figure 3 Fatigue strengths for the fin and coarse-grain versions of alloy A286.

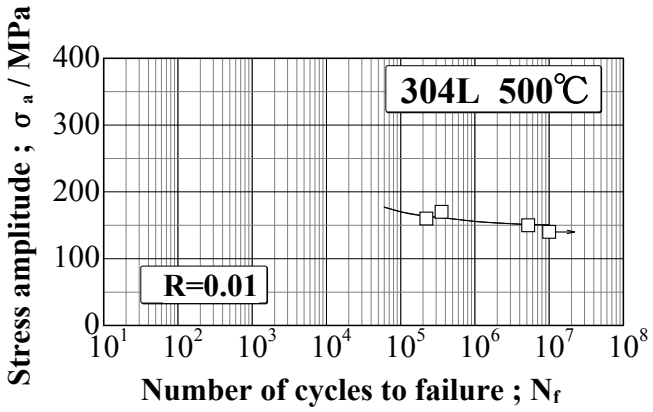

Figure 4 Fatigue strengths for the coarse-grain version of 304L steel

For alloy A286 in Figure 3, there are two test conditions of the stress ratio. Although the effect of the stress ratio naturally appears at each stress ratio, grain size effects are observed. In this case the testing temperatures were 600 ˚C for all the test conditions.

For the 304L steel in Figure 4, the fatigue strength is very low because the material is solid solution-treated and the test condition of R is 0.01. In this case the data are only for the coarse-grain version.

Fractured surfaces were observed for the specimens fractured in the low-cycle region and high-cycle region.

In the low-cycle region, the initiation site of fatigue fracture was the surface of the specimens in all the materials, as shown in Figure 5, irrespective of grain size. These fracture modes are common in the low-cycle fatigue regions in common materials as well as in alloys 718, A286 and 304L steel. Figure 5 is the case of the coarse-grain version of alloy A286. The arrow in the Figure indicates the initiation site of the fatigue fracture.

In high-cycle fatigue regions, on the other hand, the initiation site was the interior of the specimen in the coarse versions, as shown in Figure 6. Figure 6 shows a case of the coarse- grain version of alloy A286. The arrow indicates the interior initiation site of the fracture. The coarse-grain version of alloy 718 also showed the same distinct interior fracture mode in the high-cycle region. The fractured area of the initiation site is composed of many facets with crystallographic features such as in Figure 6 (b). The size of the facets is almost the same as the grain size. In the case of the coarse version of the 304L steel, the initiation site of the fracture was the surface of the specimen, since the material is not strengthened like the superalloys.

As for the fine-grain versions of alloys 718 and A286, the initiation site was also the interior. Figure 7 shows the fine-grain version of the alloy A286. The arrow in the Figure indicates the interior initiation site of the fracture. The facets with crystallographic features are also observed in the initiation area of the fracture surface, but the sizes of the facets are very small and almost the same as the fine-grain size.

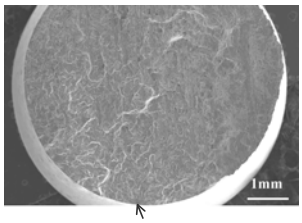

(a) Initiation site.

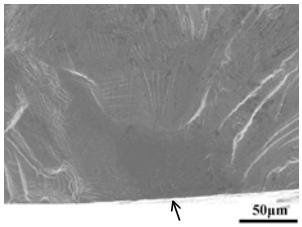

(b) High-magnification image.

Figure 5

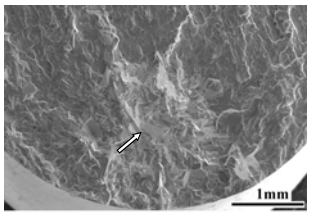

(a) Initiation site.

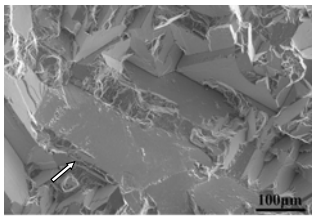

(b) High-magnification image.

Figure 6

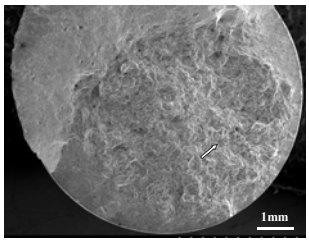

(a) Initiation site.

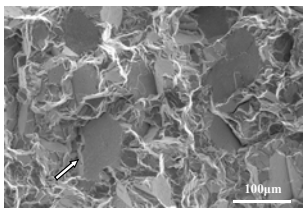

(b) High-magnification image.

Figure 7

Figure 5 Fracture surfaces fatigued in the low-cycle region for the coarse-grain alloy A286(Stress amplitude: 500MPa, N_f : 1.11×10^4 cycles, stress ratio: 0.01)

Figure 6 Fracture surfaces fatigued in the high-cycle region for the coarse-grain alloy A286(Stress amplitude: 246MPa, N_f : 5.48×10^6 cycles, stress ratio: 0.01)

Figure 7 Fracture surfaces fatigued in high-cycle region for the fine-grain alloy A286(Stress amplitude: 351MPa, N_f : 1.57×10^6 cycles, stress ratio: 0.01)

4. Discussion

Fatigue limit or fatigue strength at high-cycle region is known to correlate with tensile strength. The results of this study will be compared with reference data for various steels at high and room temperatures[5), 6), 7)].

However, there are two test conditions of the stress ratio R = –1 and 0.01, so the converted fatigue strength derived by the following equation[5)] was used.

$$\sigma_{w(R=-1)} = 1.317 \times \sigma_{w(R=0.01)} - 17.0 \quad \text{- - -} \quad \textbf{Equation (1)}$$

Where $\sigma_{w(R=-1)}$ and $\sigma_{w(R=0.01)}$ are the fatigue strength for each stress ratio. In this study the fatigue strength at 10^7 cycles was used.

Equation (1) proved to be valid for various carbon steels and austenitic steels[5)]. Using this equation makes it possible to evaluate the fatigue strength based on the common test condition of R = –1.

The relationship between the fatigue strength and the tensile strength is shown in Figure 8. All the data are under R = –1 or converted from Equation (1).

In Figure 8 the box shows the results of rotating bending fatigue tests at high temperatures for various high-temperature materials [6), 7)]. In this case, the stress ratio of R is –1 and the fatigue strength at 10^8 cycles is used. The dotted box shows the results of axial load-controlled fatigue tests for many kinds of steels with a stress ratio of R = –1 at room temperature[5)]. In this case the fatigue strength at 10^7 cycles is used. These boxes indicate the 95% confidence region.

In general, the relationship between the fatigue strength and the tensile strength is expressed as follows[5)].

$$\sigma_{w(R=-1)} = 0.5 \times \sigma_B \quad \text{- - -} \quad \textbf{Equation (2)}$$

Where $\sigma_{w(R=-1)}$ is the fatigue strength in high-cycle region and σ_B is the tensile strength.

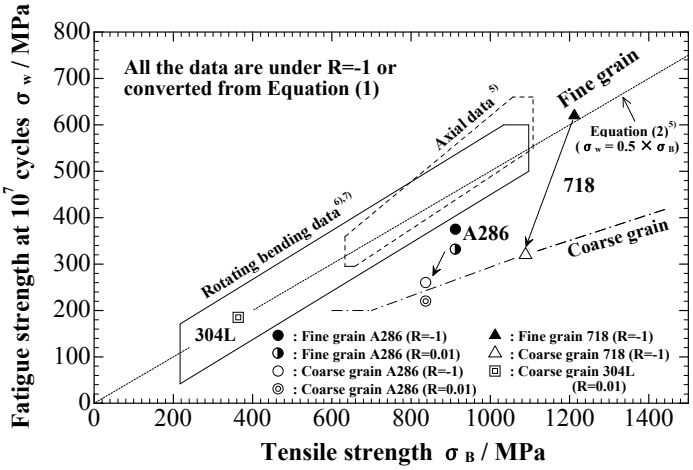

Figure 8 Relationships between fatigue strength and tensile strength

The data points such as circles, triangles and squared show the results of this study. The fatigue strength of the 304L steel tested at 500 ˚C is located in the box indicating rotating bending tests at high temperatures for conventional high-temperature materials. The data for the fine-grain versions of the alloys 718 and A286 are located in or near the boxes, and near the line of Equation (2). However, the data for the coarse-grain versions deviate from the boxes or the line of Equation (2). These deviations are discussed as follows. The reason is thought to be that the fracture site is interior, and the fracture is initiated by the large facets of the crystallographic features, and the fatigue strength is thus influenced by the size of the facets, which is almost the same as the austenitic grain size. For fine-grain materials, the fatigue strength is proportional to the tensile strength, and the strength level is almost the same as in conventional materials, such as those shown in Figure 8. Between the fine and the coarse high-strength versions, the grain size effect may appear in the fatigue strength because high-cycle fatigue strength is controlled by the facet size of the crystallographic feature at the initiation area of the fracture surface.

5. Conclusions

Fatigue strength in the high-cycle region for austenitic steel and nickel-base or iron-base superalloy were discussed from the viewpoints of austenitic gain size and tensile strength. Our conclusions are as follows.

High-strength austenitic materials with a coarse grain showed interior fractures in the high-cycle fatigue region. The initiation site was composed of various large facets of the crystallographic features and the facets were as large as the grain size. So the fatigue strength deviated from the equation line of $\sigma_{w(R=-1)} = 0.5 \times \sigma_B$ in the relationship between $\sigma_{w(R=-1)}$ and σ_B, where $\sigma_{w(R=-1)}$ was the fatigue strength under the stress ratio R of –1, and σ_B was the tensile strength.

On the other hand, high-strength austenitic materials with a fine grain also showed interior fractures in the high-cycle fatigue region. However, the facets at the initiation sites were as small as the fine grain size. The fatigue strength was therefore at almost the same level as in conventional materials, which obey the equation of $\sigma_{w(R=-1)} = 0.5 \times \sigma_B$.

From the above rationale, the high-cycle fatigue strength for high-strength austenitic steel or superalloys is determined by the austenitic gain size and the tensile strength, since the high-cycle fatigue strength is controlled by the facet size of the crystallographic features at the initiation area on the fracture surface.

References

1) NIMS Space Use Materials Strength Data Sheet No.0 (National Institute for Materials Science, Tsukuba, 2003)
2) NIMS Space Use Materials Strength Data Sheet No.4 (National Institute for Materials Science, Tsukuba, 2004)
3) NIMS Space Use Materials Strength Data Sheet No.6 (National Institute for Materials Science, Tsukuba, 2005)

4) NIMS Space Use Materials Strength Data Sheet No.7 (National Institute for Materials Science, Tsukuba, 2006)
5) S.Nishijima, A.Ishii, K.Kanazawa, S. Matsuoka and C.Masuda: NRIM Material Strength Data Sheet Technical Document, No.5, National Research Institute for Metals, Tokyo, (1989), 53.
6) S.Yoshida, K.Kanazawa, K.Yamaguchi, M.Sasaki, K. Kobayashi and M.Sato, Trans. National Research Institute for Metals, Tokyo, **19**, 247 (1977)
7) K.Kanazawa, K.Yamaguchi and S.Sato: NRIM Material Strength Data Sheet Technical Document, No.6, National Research Institute for Metals, Tokyo, (1990), 28